12,19

Catastrophic destruction of carbon nanotubes during degradation of field emitters

© *S.V. Bulyarskiy, A.A. Dudin, A.V. Lakalin, A.P. Orlov*

Institute of Nanotechnology of Microelectronics, Russian Academy of Sciences,
Moscow, Russia

E-mail: bulyar2954@mail.ru

The catastrophic degradation of emission cathodes based on carbon nanotubes is simulated, which occurs due to the destruction of the nanotube in the defective region as a result of overheating. The model takes into account the heating of the nanotube by releasing Joule heat, as well as radiation and cooling due to the Notingham effect, which consists in reducing the temperature of the emitting end due to the energy carried away by the flow of emitted electrons. The proposed model is compared with an experiment on the degradation of a single nanotube. The experiment confirms the catastrophic destruction and shows that the destruction is facilitated by the occurrence of thermoelectronic emission, which causes a rapid increase in the current and, accordingly, the temperature of the defective region of the nanotube.

Keywords: field emitters, degradation, nanotube heating, defects, catastrophic destruction.

1. Introduction

The use of carbon nanotubes (CNT) as a material for field emitters has started almost immediately after their emergence [1,2]. The research is this area was underway due to creation of new CNT-based devices: display units [3], miniature X-ray tubes [4,5], LEDs [6], THz-band amplifiers [7,8], fast-acting vacuum switches [9], electrical motion systems [10].

Despite the wide application prospects of the CNT-based field emitters, the process is hampered by the limited service life due to their fast degradation. Stability of these devices and causes of their degradation have not been still adequately investigated. Emission current stability is usually measured during 24 h, which is obviously insufficient for practical application and equipment behavior during service life is rarely studied [11–13].

Various methods are used for field emission cathode current stabilization. For example, instead of CNT bundles evenly distributed over the surface, carbon fibers [14,15] are used and demonstrate higher stability compared with vertical nanotube arrays. To increase the emission current stability, matrix field emission cathodes consisting of vertical nanotubes about one micron in diameter or smaller. Such design reduces electric field weakening thanks to shielding by the adjacent nanotubes and improves their cooling. Moreover, for emission stabilization, artificial ageing of field emission cathodes is performed at high dc current densities during a specified period of time [16,17]. DC current flowing through the CNT body during operation as an emitter causes CNT heating [18]. Though the emitting nanotube end is cooled due to the Nottingham effect, overheating may be high achieving thousands of degrees.

At such temperature, nanotube failure starts due to carbon evaporation from the surface. It should be noted that CNT included in the bundle have various length. Ends of long nanotubes are placed closer to the anode and electric field in this area is higher. Therefore, current in long tubes is higher than in short ones. They are heated more intensively and decay faster. The nanotube bundle is straightened by current ageing and cathode current is stabilized. The mechanism behind the nanotube shortening is still studied inadequately. The mere nanotube substance evaporation shall not cause fast changes in nanotube dimensions such as observed in practice. Catastrophic nanotube failure occurs when the nanotube end, whose dimensions constitute a considerable part of the nanotube, is broken. Such nanotube failure is indicative of its nonuniform heating. Temperature distribution along the nanotube provided that this tube has uniform resistance is calculated in [18]. However, the carbon nanotube morphology analyses detect defective areas of various origin which shall result in nonuniform resistance of a tube body. The purpose of this paper is to clarify the influence of defective areas in nanotubes with high electric resistance on catastrophic failure of nanotubes during high current flow.

2. Defective carbon nanotube heating

Electric current causes CNT heating. This heating is nonuniform. When a carbon nanotube is used as a field emitter, then it is in vacuum and is attached with its one end to the substrate through which heat is removed. The substrate has high surface area and weight, therefore the attached nanotube end may be considered to have the substrate temperature. Heat is also removed due to emission from the CNT side surface. Nevertheless,

the nanotube temperature tends to increase towards the nanotube end [18]. However, the end itself is cooled due to the Nottingham effect that is associated with the loss of energy carried over by the emitted electron flow [18,19]. Therefore the nanotube temperature maximum occurs at a distance from the emitting end [18]. The presence of high-resistance defective nanotube areas shall cause additional heating of CNT. To show this effect, CNT with three high-resistance defective areas were addressed.

For simulation, additional resistivities of defective areas were established by Gaussian functions:

$$\xi_i(x) = \rho_i \exp\left(-\frac{(x - \mu_i)^2}{2\gamma_i^2}\right), \tag{1}$$

where $\xi_i(x)$ is the distribution of additional resistivity throughout CNT induced by the i-th defect ($i = 1, \ldots, n$, where n is the number of defects); ρ_i is the additional resistivity in the i-th defect area; μ_i is the position of the i-th defect center; γ_i is the distribution dispersion of a defective area that was considerably lower than the CNT length.

Total resistivity of CNT, including distribution over positions and temperature dependence, will be written as

$$\rho(x, T) = \left(\rho_0 + \sum_{i=1}^{n} \rho_i \exp\left(-\frac{(x - \mu_i)^2}{2\gamma_i^2}\right)\right)$$
$$\times (1 - \alpha T + \beta T^{3/2}), \tag{2}$$

where ρ_0 is the constant component of the CNT body resistivity; α and β are resistivity temperature coefficients.

Simulation was carried out by solution of the non-steady-state heat conduction equation

$$k_0 \frac{\Theta}{T}\left(\frac{\partial^2 T}{\partial x^2} - \frac{1}{T}\left(\frac{\partial T}{\partial x}\right)^2\right) - \frac{2\pi r}{S}\eta\sigma(T^4 - T_0^4)$$
$$+ I^2 \frac{\rho(x, T)}{S^2} = \rho_{dens} c_{sp} \frac{\partial T}{\partial t}, \tag{3}$$

where r is the external radius of CNT; S is the CNT cross-section ($S = \pi r^2$), $k(T) = k_0 \frac{\Theta}{T}$ is the thermal conductivity coefficient along the CNT axis [19], $T = T(x, t)$ is the temperature along the CNT axis, T_0 is the substrate temperature, $\rho(x, T)$ is the CNT resistivity, η is the thermal radiation greyness value of CNT ($\eta < 1$), $\sigma = 5.67 \cdot 10^{-8} \, \mathrm{W/(m^2 \cdot K^4)}$ is the Stefan−Boltzmann constant, I is the current flowing through CNT, Θ is the Debye temperature, ρ_{dens} is the CNT density, c_{sp} is the CNT specific heat capacity.

The first term of equation (3) account for the heat flow through CNT as a result of a temperature gradient along the nanotube, the second term accounts for heat removal due to thermal radiation from the side surface, and the third term is responsible for heat release caused by the current flow.

Heat conduction equation (3) was added with the following initial and boundary conditions

$$T(0, t) = k_0 \frac{\Theta}{T(0, t)} \lambda S \frac{\partial T(0, t)}{\partial x} + T_0,$$

$$\frac{\partial T(L, t)}{\partial x} = -\left(k_0 \frac{\Theta}{T(L, t)}\right)^{-1} \eta\sigma\left(T^4(L, t) - T_0^4\right)$$
$$- \left(k_0 \frac{\Theta}{T(L, t)}\right)^{-1} \frac{3k_B T(L, t)}{2} \frac{I}{qS}, \tag{4}$$
$$T(x, 0) = T_0,$$

where L is the CNT length, k_B is the Boltzmann constant, q is the elementary charge, λ (K/W) is the integral coefficient describing the dependence of the temperature of the secured end on the contact resistance between CNT and substrate and on other properties. For establishing the CNT position, the end attached to the substrate was in point $x = 0$, while the emitting end was in point $x = L$. With $\lambda = 0$, a simple boundary condition version $T(0, t) = T_0$ is derived, when the temperature of the attached CNT end will be equal to that of the substrate body.

As will be explained in the experimental setup description in the next Section, the electrode to which CNT is attached is much heavier than the tube itself. CNT was attached to this electrode, made in the form of a tungsten needle, by means of local platinum sputtering induced by an electron beam in a microscope chamber when reliable mechanical strength and low contact resistance were ensured. Therefore, for the purpose of calculations, $\lambda = 0$ was assumed at the boundary $x = 0$ and, thus, condition $T(0, t) = T_0$ was used.

Equation (3) with initial and boundary conditions (4) and specific resistance (2) was solved numerically with the following coefficients:

$$\alpha = 8.5 \cdot 10^{-4} \, \mathrm{K^{-1}}, \quad \beta = 9.8 \cdot 10^{-6} \, \mathrm{K^{-3/2}}, \quad \lambda = 0,$$

$$\rho_0 = 3.26 \cdot 10^{-5} \, \Omega \cdot \mathrm{m}, \quad L = 2 \, \mu\mathrm{m}, \quad r = 7 \, \mathrm{nm}, \quad T_0 = 300 \, \mathrm{K},$$

$$I = 10 \, \mu\mathrm{A}, \quad \Theta = 1190 \, \mathrm{K}, \quad k_0 = 25.21 \, \mathrm{W/(m \cdot K)}, \quad \eta = 0.9,$$

$$\rho_{dens} = 1400 \, \mathrm{kg/m^3}, \quad c_{sp} = 710 \, \mathrm{J/(kg \cdot K)},$$

$$\rho_1 = \rho_2 = \rho_3 = 10\rho_0 = 3.26 \cdot 10^{-4} \, \Omega \cdot \mathrm{m},$$

$$\gamma_1 = \gamma_2 = \gamma_3 = 0.01L = 0.02 \, \mu\mathrm{m},$$

$$\mu_1 = 0.3L = 0.6 \, \mu\mathrm{m}, \quad \mu_2 = 0.5L = 1.0 \, \mu\mathrm{m},$$

$$\mu_3 = 0.7L = 1.4 \, \mu\mathrm{m}.$$

The obtained solution for the CNT temperature distribution in various points of time is shown in Figure 1. Positions of singularities on the curves correspond to positions μ_i local defect center positions.

The calculation shows that after energizing the nanotube is gradually heated. temperature distribution features are observed in defective areas, and the absolute maximum with time may be achieved at different distances from the substrate while gradually moving to the emitting nanotube end. The temperature achieves its critical level in one of the defective areas with an increase in current. In this area, the nanotube may evaporate at a higher rate and may get broken which is the cause of catastrophic degradation.
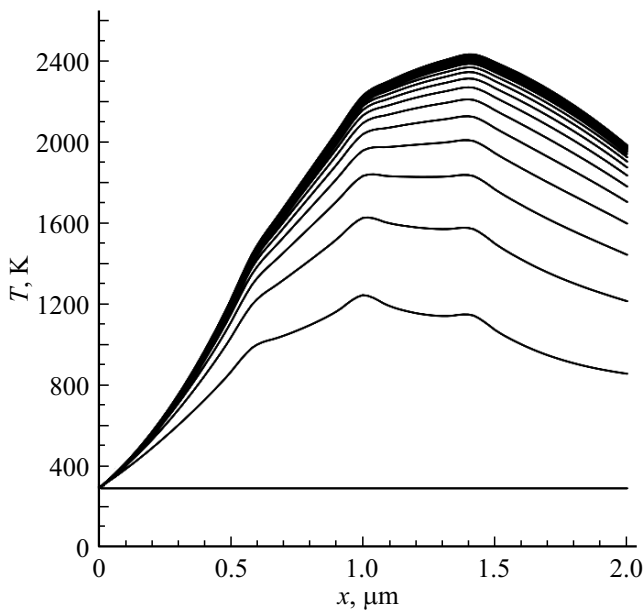
Figure 1. temperature distribution along CNT in time interval $t = 0 - 10^{-7}$ s with increment $\Delta t = 5 \cdot 10^{-9}$ s at $I = 10 \,\mu$m in presence of three local point defects.
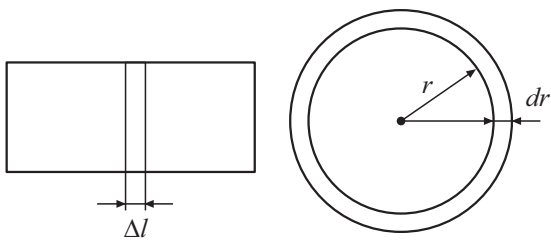
Figure 2. CNT length element.

Carbon evaporation from the CNT surface in vacuum may be considered using the Hertz−Knudsen law [20]:

$$J = p_S(T) \sqrt{\frac{m_0}{2\pi k_B T}}, \qquad (5)$$

where J is the mass flux of the evaporated substance ($kg/(s \cdot m^2)$); $J = \frac{1}{\Delta S} \frac{dm}{dt}$; ΔS is the area from which evaporation takes place; dm is the weight of the evaporated substance per time dt; m_0 is the atomic weight of the evaporated substance (carbon); $p_s(T)$ is the pressure of saturated substance (carbon) vapor at absolute temperature T.

Dependence of the saturated vapor pressure vs. temperature may be described, for example, as follows [21]:

$$p_S(T) = 1.36943 \cdot 10^{13} \exp\left(-\frac{80472.5}{T}\right), \qquad (6)$$

where temperature T is measured in K, pressure p_S is measured in Pa.

The Hertz−equation shall be associated with the CNT parameters. Consider CNT length element Δl (Figure 2). During time dt, a thin carbon layer with thickness dr was evaporated from the surface of this element.

CNT weight will change by $dm_{CNT} = \rho_{dens} dV = \rho_{dens} dS \Delta l = \rho_{dens} 2\pi r dr \Delta l$. Then, taking into account $dm = -dm_{CNT}$, the following weight of the evaporated carbon is derived

$$dm = -\rho_{dens} 2\pi r dr \Delta l. \qquad (7)$$

On the other hand, according to the Hertz−Knudsen equation (5), carbon with weight

$$dm = \Delta S_\Omega p_S(T) \sqrt{\frac{m_0}{2\pi k_B T}} \, dt$$

$$= 2\pi r \Delta l \, p_S(T) \sqrt{\frac{m_0}{2\pi k_B T}} \, dt. \qquad (8)$$

was evaporated from the side surface of this element ΔS_Ω By equation of (7) and (8), we obtain

$$\frac{\partial r}{\partial t} = -\frac{1}{\rho_{dens}} p_S(T) \sqrt{\frac{m_0}{2\pi k_B T}}. \qquad (9)$$

Here, $r = r(x, t)$, $T = T(x, t)$. Initial condition for r will be $r(x, 0) = r_0$, where r_0 is the initial CNT radius before heating.

To describe the process of carbon evaporation from CNT in vacuum, equation (9) and non-steady-state heat conduction equation (3) shall be solved together.

Finally, the following system of two differential equations with initial and boundary conditions is derived:

$$k_0 \frac{\Theta}{T} \left(\frac{\partial^2 T}{\partial x^2} - \frac{1}{T} \left(\frac{\partial T}{\partial x} \right)^2 \right) - \frac{2}{r} \eta \sigma (T^4 - T_0^4)$$

$$+ \frac{I^2}{(\pi r^2)^2} \left(\rho_0 + \sum_{i=1}^{n} \rho_i \exp\left(-\frac{(x - \mu_i)^2}{2\gamma_i^2} \right) \right)$$

$$\times (1 - \alpha T + \beta T^{3/2}) = \rho_{dens} c_{sp} \frac{\partial T}{\partial t},$$

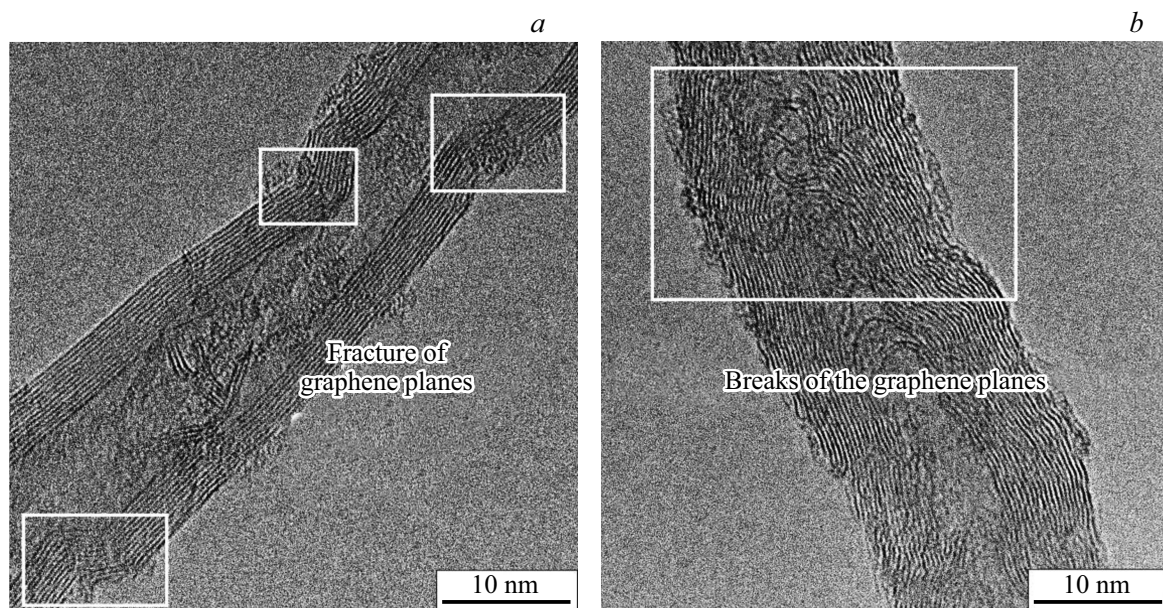$$T(0, t) = k_0 \frac{\Theta}{T(0, t)} \lambda S \frac{\partial T(0, t)}{\partial x} + T_0,$$

$$\frac{\partial T(L, t)}{\partial x} = -\left(k_0 \frac{\Theta}{T(L, t)} \right)^{-1} \eta \sigma (T^4(L, t) - T_0^4)$$

$$- \left(k_0 \frac{\Theta}{T(L, t)} \right)^{-1} \frac{3 k_B T(L, t)}{2} \frac{I}{qS},$$
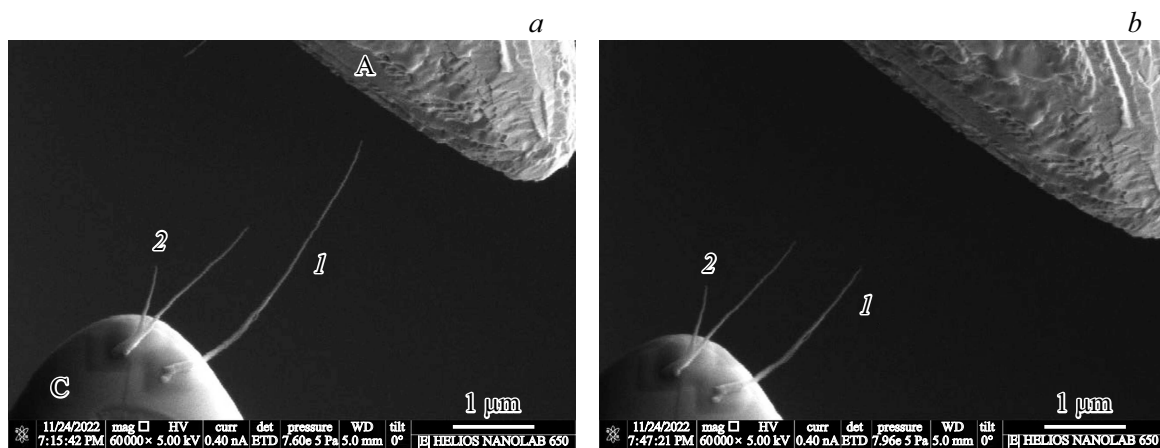
$$T(x, 0) = T_0,$$

$$\frac{\partial r}{\partial t} = -\frac{1}{\rho_V} p_S(T) \sqrt{\frac{m_0}{2\pi k_B T}},$$

$$r(x, 0) = r_0, \qquad (10)$$

where $r = r(x, t)$, $T = T(x, t)$. Therefore, system (10) fully describes the temperature variation process along CNT and radius reduction as a result of carbon evaporation from the CNT surface.

Figure 3. Images of multilayer carbon nanotubes with macroscopic defects: *a*) fracture of the graphene planes; *b*) breaks of the graphene planes.


Figure 4. emission system image in the scanning-electron microscope with the attached nanotube (*1*) via which the emitting current flows: (*a*) immediately after creation; (*b*) after catastrophic degradation of the nanotube (*1*) caused by heating at high current. The Figure also shows the images of nondegraded nanotubes (*2*).

3. Experimental verification of the catastrophic degradation model

For experimental verification of the catastrophic degradation model of CNT, a setup was assembled consisting of FEI HeliosNanoLab 650 DualBeam scanning electron/ion microscope with Kleindiek MM3A-EM nanomanipulator system. Emission characteristics were measured using Keithley 2634B programmable two-channel source meter capable of generating and measuring voltage and current with low noise level. According to the original procedure [22], a single carbon nanotube was extracted from the vertical array using the electronic microscope arms and attached to the tungsten needle tip.

Carbon nanotube arrays were grown on silicon substrates. Synthesis was carried out at $700°C$ with nickel catalyst composed of acetylene, ammonia and argon mixture with ratio: $1:1:3$. Figure 3 shows the images of single nanotubes made using a high-resolution transmission electron microscope. The tubes were multilayer with the number of walls varying from 15 to 25, they contained macroscopic defects also shown in Figure 3. The specified defects may induce high resistance regions.

The tungsten needle with CNT attached to it served as a cathode (C), and nanotube served as emitter from which electrons were emitted. A sharp needle tip on the second arm placed at a small distance (with gap $< 500\,nm$) served as anode (A), see Figure 4, *a*.
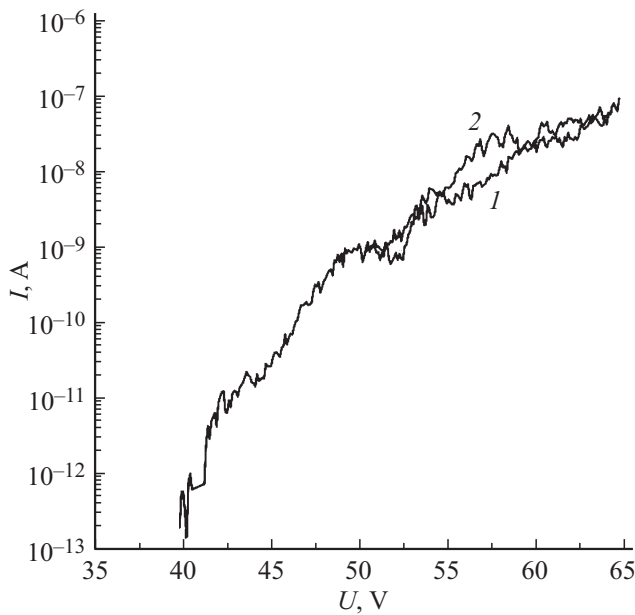
Figure 5. current-voltage characteristic of cathode–CNT–anode system shown in Figure 3: *1* — with voltage increase from 0 to U_{max}; *2* — with voltage decrease from U_{max} to 0.

Cathode-anode current-voltage characteristic was measured in high-vacuum chamber of the microscope in two modes. The first mode involved the emission current-voltage characteristic measurement with smooth voltage increase up to the maximum level limited by current, and then voltage decrease to zero (for the experiment, the limiting current set to about 100 nA). The second mode used step-like current increase up to emission limits for a single CNT. The power supply was operated as a current source to maintain permanent current within approximately one minute and then the current was increased in a step-like manner. The holding time was defined by the CNT voltage stabilization that varied with transition to a next current level, and then was stabilized at a new level. At a step when the limit current was achieved, CNT got broken as a result of critical overheating of one of the defective regions. Figure 4, *b* shows how the distance from the nanotube end to the anode varied in this case. After CNT failure, electric field strength at the new emitting end dropped dramatically and the current decreased almost to zero. This is the essence of catastrophic degradation.

The current-voltage characteristic in the first mode was measured between the cathode and anode and is shown in Figure 5. Curve *1* — current-voltage characteristic with voltage increase from zero to U_{max}, and curve *2* — reversed voltage measurement from U_{max} to zero. The results show that the emission current-voltage characteristic has a hysteresis that may be associated with heating of the sample. This is indicated by the increase in current on curve *2* compared with curve *1*.

Sample resistance is certainly grows with nanotube heating, because resistivity grows with temperature, therefore, current should have dropped. However, the total current is defined not only by the nanotube body resistance, but also by the resistance at the vacuum interface. This resistance is defined, on the one hand, by tunneling of electrons under the potential barrier that occurs at the nanotube-vacuum boundary due to work function, and, on the other hand, by thermoelectron emission above the potential barrier [18]. These resistances are connected in parallel and in series with the nanotube body resistance. During heating, the probability of thermoelectron emission grows, while equivalent resistance of this process and total resistance at the vacuum interface drops. Thus, the current increase is associated with thermoelectron emission. Heating grows with current increase, the process has an avalanche-like increase and the tube breaks at the maximum overheating point as shown in Figure 4, *b*.

The experimental characteristic of the second mode is shown in Figure 6. For this experiment, the power supply was connected in the current setting mode with current increased in a step-like manner from $1\,\mu A$ to $13.5\,\mu A$ with increment $0.5\,\mu A$. A delay of 1 min was used at each current step, which was enough for nanotube heating. Catastrophic degradation occurred at 1513-th second (vertical line) at current $13.5\,\mu A$.

This experiment was simulated using the derived system of equations (10).

According to the SEM image (Figure 4), CNT had the following geometrical values: initial length $3\,\mu m$, length after degradation $2\,\mu m$, mean radius 15 nm. Since the temperature achieves its maximum in the defect point, then an assumption was made that the CNT failure occurred exactly in this point. Therefore, CNT with a single defect ($n = 1$) with $\rho_1 = 13.5\rho_0 = 4.401 \cdot 10^{-4}\,\Omega \cdot m$, $\sigma_1 = 0.03\,\mu m$, $\mu_1 = 2\,\mu m$ was addressed. For solution of
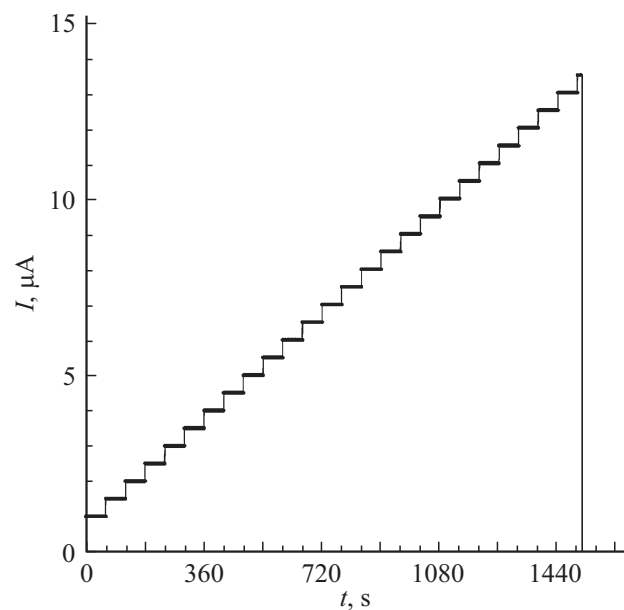
Figure 6. Time-current curve with step-like current increase with time delay at each step 60 s. Catastrophic degradation occurred at 1513th second (vertical line).
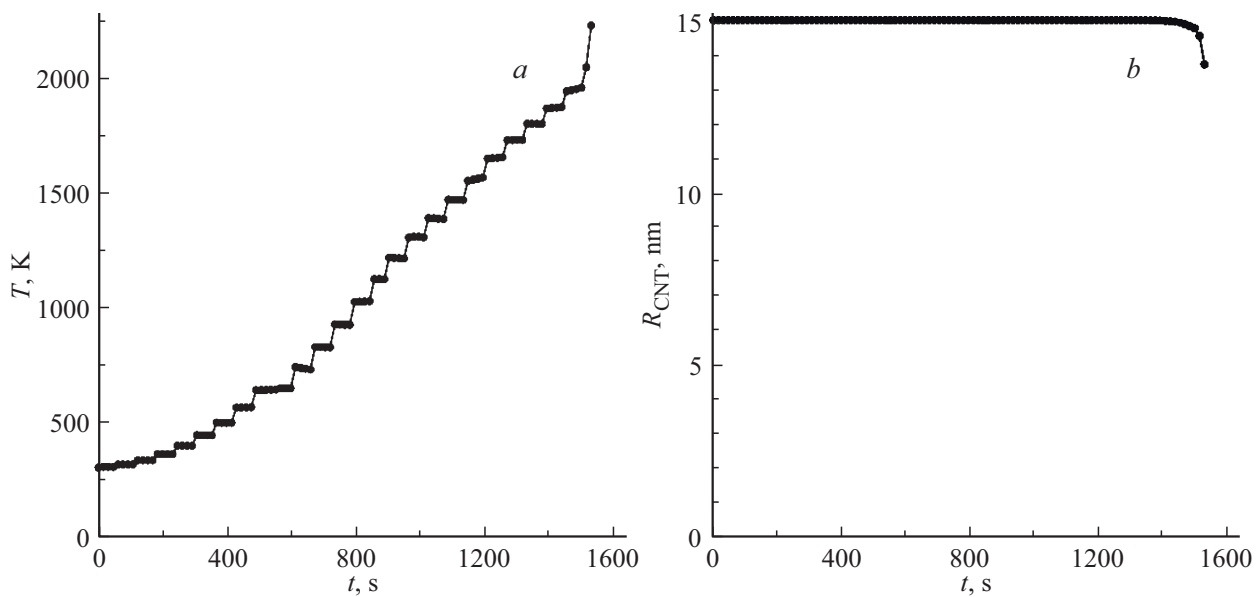
Figure 7. The calculated dependences of temperature (*a*) and CNT radius (*b*) vs. time in point $x \approx 2.0\,\mu$m for the experiment with step-like current sweep.

system (10), other coefficients were set as shown above. As a result, time to CNT failure was calculated: $t \approx 1526$ s. This value was rather close to the experimental value. Figure 7 shows dependences $T(t)$ and $r(t)$ calculated for point $x \approx 2.0\,\mu$m in the vicinity of which the failure has occured. It can be seen that CNT radius reduction and temperature increase at 1526-th second develop in an avalanche-like manner.

4. Conclusions

Based on the calculations and experiments, the following conclusions may be made.

1. The Nottingham effect causes cooling of the emitting CNT end. As a result, a region with the highest temperature containing the maximum temperature point at a distance from the edge is found.

2. The presence of local defective regions and appropriate CNT resistance result in the increase in temperature of the whole CNT and temperature distribution singularities in the vicinity of defects.

3. Catastrophic degradation of CNT in vacuum occurs as follows. CNT is heated nonuniformly. In the defective region, the temperature is higher. With temperature increase, nanotube substance evaporation from the surface may occur.

The avalanche-like temperature growth is caused by thermoelectron emission that reduces resistance in the cathode−anode space. This increases the current, with thermoelectron emission current increasing first, etc. Fast temperature growth occurs from one of the defective regions which is usually located closer to the emitting end. Overheating may achieve carbon evaporation temperatures from the nanotube surface and this is one of the causes of

degradation. It is important that heating occurs exactly in these defective regions. Therefore, heating is uneven and the tube may be broken exactly in the points of defects, which is observed in the operation process.

Conflict of interest

The authors declare that they have no conflict of interest.

References

[1] L.A. Chernozatonskii, Y.V. Gulyaev, Z.J. Kosakovskaja, N.I. Sinitsyn, G.V. Torgashov, Y.F. Zakharchenko, E.A. Fedorov, V.P. Val'chuk. Chem. Phys. Lett. **233**, *1–2*, 63 (1995). https://doi.org/10.1016/0009-2614(94)01418-U

[2] W.A. de Heer, A. Châtelain, D. Ugarte. Science **270**, *5239*, 1179 (1995). https://doi.org/10.1126/science.270.5239.1179

[3] M. Mauger, V.T. Binh. J. Vac. Sci. Technol. B **24**, *2*, 997 (2006). https://doi.org/10.1116/1.2179454

[4] A.P. Gupta, S. Park, S.J. Yeo, J. Jung, C. Cho, S.H. Paik, H. Park, Y.C. Cho, S.H. Kim, J.H. Shin, J.S. Ahn, J. Ryu. Materials **10**, *8*, 878 (2017). https://doi.org/10.3390/ma10080878

[5] S. Park, A.P. Gupta, S.J. Yeo, J. Jung, S.H. Paik, M. Mativenga, S.H. Kim, J.H. Shin, J.S. Ahn, J. Ryu. Nanomaterials **8**, *6*, 378 (2018). https://doi.org/10.3390/nano8060378

[6] M. Croci, I. Arfaoui, T. Stöckli, A. Chatelain, J.-M. Bonard. Microelectronics J. **35**, *4*, 329 (2004). https://doi.org/10.1016/j.mejo.2003.07.003

[7] C. Paoloni, M. Mineo, A. Di Carlo, A.J. Durand, V. Krozer, M. Kotiranta, F. Bouamrane, T. Bouvet, S. Megtert. In: Proc. 2012 IEEE Thirteenth Int. Vacuum Electron. Conf. (IVEC). Monterey, CA, USA. 24−26.04.2012. IVEC (2012) (IEEE). P. 237−238.

[8] H.Y. Yuan, X.R. Wang. Sci. Rep. **6**, 22638 (2016). https://doi.org/10.1038/srep22638

[9] N.L. Rupesinghe, M. Chhowalla, K.B.K. Teo, G.A.J. Amaratunga. J. Vac. Sci. Technol. B **21**, *1*, 338 (2003). https://doi.org/10.1116/1.1527635

[10] I. Levchenko, S. Xu, G. Teel, D. Mariotti, M.L.R. Walker, M. Keidar. Nature Commun. **9**, *1*, 879 (2018). https://doi.org/10.1038/s41467-017-02269-7

[11] B. Galante, G.A. Tranquille, M. Himmerlich, C.P. Welsch. J. Resta López. Phys. Rev. Accel. Beams **24**, *11* (2021). https://doi.org/10.1103/PhysRevAccelBeams.24.113401

[12] N.T. Hong, K.H. Koh, S. Lee, P.N. Minh, N.T.T. Tam, P.H. Khoi. J. Vac. Sci. Technol. B **27**, *2*, 749 (2009). https://doi.org/10.1116/1.3097850

[13] J.T.L. Thong, C.H. Oon, W.K. Eng, W.D. Zhang, L.M. Gan. Appl. Phys. Lett. **79**, *17*, 2811 (2001). https://doi.org/10.1063/1.1412590

[14] S.B. Fairchild, P. Zhang, J. Park, T.C. Back, D. Marincel, Z. Huang, M. Pasquali. IEEE Trans. Plasma Sci. **47**, *5*, 2032 (2019). https://doi.org/10.1109/TPS.2019.2900219

[15] Y. Guo, J. Wang, B. Li, Y. Zhang, S. Deng, J. Chen. Nanomaterials **12**, *11*, 1882 (2022). https://doi.org/10.3390/nano12111882

[16] J.H. Kim, J.S. Kang, K.C. Park. Micromachines **9**, *12*, 648 (2018). https://doi.org/10.3390/mi9120648

[17] J.H. Ryu, K.S. Kim, C.S. Lee, J. Jang, K.C. Park. J. Vac. Sci. Technol. B **26**, *2*, 856 (2008). https://doi.org/10.1116/1.2884757

[18] S.V. Bulyarskiy, A.A. Dudin, A.V. Lakalin, A.P. Orlov, A.A. Pavlov, R.M. Ryazanov, A.A. Shamanaev. Tech. Phys. **63**, *6*, 894 (2018). https://doi.org/10.1134/S1063784218060099

[19] J. Paulini, T. Klein, G. Simon. J. Phys. D **26**, *8*, 1310 (1993). https://doi.org/10.1088/0022-3727/26/8/024

[20] J.P. Hirth, G.M. Pound. Condensation and Evaporation: Nucleation and Growth Kinetics. Macmillan, N.Y. (1963). 191 p.

[21] K.P. Shumsky, A.I. Myalkin, I.S. Maksimovskaya. Osnovy rascheta vakuumnoi sublimatsionnoy apparatury. Mashinostroenie, M. (1967), 224 p. (in Russian).

[22] A.A. Dudin, A.P. Orlov, E.V. Zenova, A.M. Tagachenkov. NMST **20**, *9*, 515 (2018). https://doi.org/10.17587/nmst.20.515-520.

Translated by E.Ilyinskaya